SELECTIVE LASER SINTERING OF NEGATIVE STIFFNESS MESOSTRUCTURES FOR RECOVERABLE, NEARLY-IDEAL SHOCK ISOLATION

Timothy Klatt, Michael Haberman, and Carolyn Conner Seepersad
Department of Mechanical Engineering and Applied Research Laboratories
University of Texas at Austin

ABSTRACT

Honeycomb materials are well known for providing lightweight stiffness, strength, and energy absorption capabilities. For most honeycomb materials, energy absorption occurs when individual cells collapse progressively. Although it is possible for honeycombs with very low relative density to collapse via elastic buckling, honeycombs with typical relative densities collapse due to plastic yielding and buckling of the cell walls, such that the energy absorption is nonrecoverable. In this paper, mono-stable negative stiffness unit cells are investigated for constructing honeycomb mesostructures with high levels of recoverable energy absorption. Negative stiffness is achieved by incorporating curved beams into each unit cell. When subject to transverse loading, the curved beams exhibit negative stiffness behavior as they transition from one curved geometry to another in a snap-through type of motion that absorbs energy elastically at a relatively constant plateau stress. The plateau stress at which this energy absorption occurs can be tailored via the geometry of the unit cell. Preliminary experiments indicate that the structures can absorb significant amounts of energy by requiring nearly-constant-force to increase deformation as the structure transitions between snap-through configurations. Unlike traditional honeycombs, the negative stiffness mesostructures are self-resettable and therefore reusable. Using SLS as a means of fabrication, they can also be customized for specific shock events and even functionally graded to offer shock isolation for transient loads of various amplitudes.

Keywords: bistable structures, mesostructures, honeycombs, selective laser sintering

1. INTRODUCTION TO POSITIVE AND NEGATIVE STIFFNESS HONEYCOMB MESOSTRUCTURES

Honeycomb materials are well-known for lightweight stiffness, strength, and mechanical energy absorption [1]. When subjected to in-plane compression, honeycomb structures typically undergo an initial region of elastic deformation, in which the cell walls bend, compress, and/or extend elastically. The stiffness depends on the cell structure, with the in-plane effective elastic stiffnesses of several standard cell structures illustrated in Figure 1. As shown in Figure 2, the region of elastic deformation typically ends when the mesostructure reaches a plateau stress, at which point the individual cell walls begin to collapse by buckling. At extremely low relative densities, elastic buckling can occur, but for most practical relative densities, collapse is associated with plastic buckling and yielding. The mesostructure continues to absorb energy as cell walls progressively collapse, defining the plateau region in Figure 2. Eventually, when cell wall collapse is complete, the mesostructure densifies, and stiffness rapidly approaches that of the constituent material in the cell walls. This stress-strain behavior has been documented for several cell structures (cf. [1,2]).

One interesting aspect of the stress-strain curve in Figure 2 is that it corresponds very closely to that of an ideal shock isolator from structural dynamics. An ideal shock isolator provides a constant force response to an applied shock loading and thereby absorbs a maximum amount of input energy for a given displacement and allowable force transmitted to the isolated mass [3-5]. To achieve this effect, it typically exhibits linear stiffness in response to an applied force, until the force reaches a predesigned force threshold, at which point the ideal shock isolator absorbs energy at a constant force level, also known as a quasi-zero stiffness regime. One of the advantages of this type of isolator is that it acts as a force switch—absorbing significant amounts of energy at a particular force threshold and protecting the isolated structure from forces or accelerations beyond that threshold. An ideal system would then return to equilibrium when the applied load is released in preparation for the next shock.

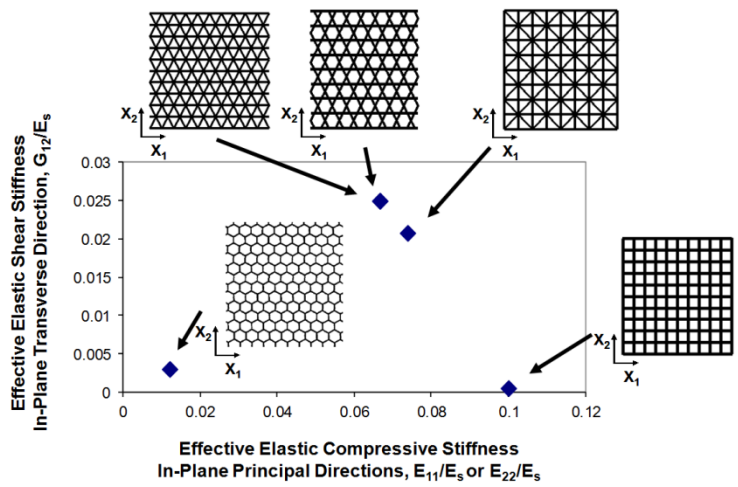

Figure 1. Effective elastic properties of standard periodic cellular topologies (courtesy of [6]).

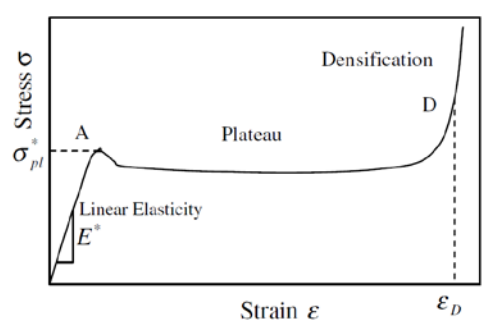

Figure 2. Stress-strain curve for a typical honeycomb structure under in-plane compression, illustrating a characteristic plateau region of mechanical energy absorption (courtesy of [2]).

One way to achieve nearly ideal shock isolation in practice is to use negative stiffness structures. Bistable structures, such as an axially compressed, buckled beam, are examples of negative stiffness elements because they exhibit negative stiffness behavior as they transition between two stable states. An illustration of a buckled beam is shown in Figure 3. States (1) and (3) in Figure 3 represent the bistable states of the beam. A representative constitutive curve for a

buckled beam is shown in Figure 4. States (1), (2), and (3) in Figure 4 correspond to those in Figure 3. State (2) represents an unstable equilibrium, also called a meta-stable state. In the meta-stable state, no external force is required to hold the beam in the configuration, but the second derivative of the beam's strain energy with respect to displacement is negative. As a result, the beam is unstable and any minor perturbation causes the beam to seek one of the two stable states, (1) or (3), unless an additional constraint is applied. As shown in Figure 4, a region of negative slope, or negative stiffness, exists between the two bistable states. The region of negative stiffness is centered about the meta-stable state of the beam. When an axially compressed beam transits from one stable state to another, its negative stiffness can be tuned to balance the positive stiffness of a spring in parallel with it, resulting in a region of constant force response, also known as a quasi-zero stiffness regime [7].

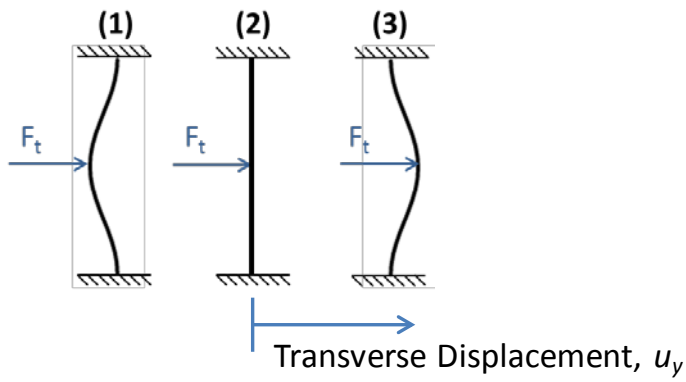

Figure 3. First-mode buckled beam transitioning from one stable state to another under transverse loading, F_t.

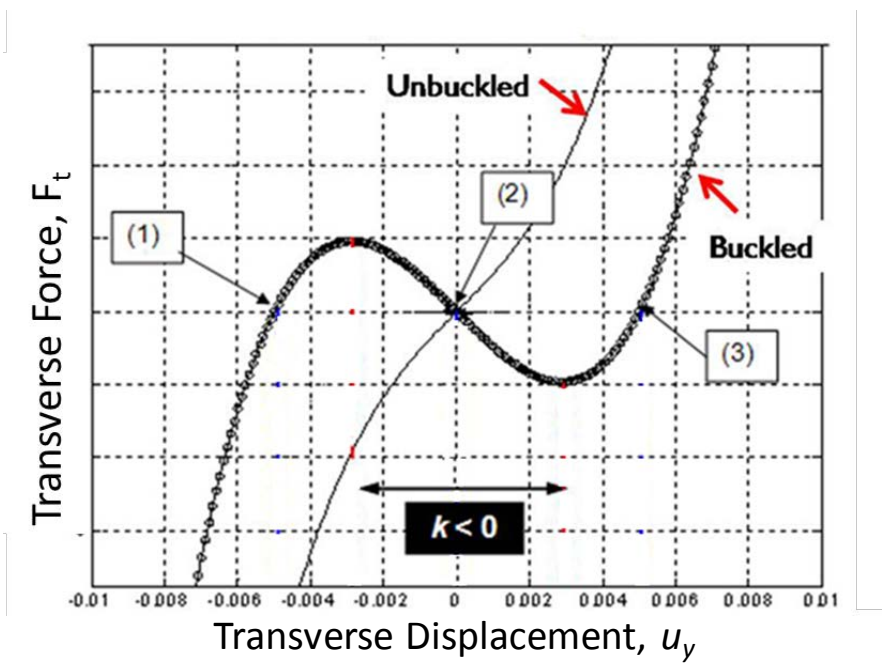

Figure 4. Transverse constitutive relationship of an axially compressed, buckled beam, relative to that of an unbuckled beam.

While axially compressed beams work well as negative stiffness mechanisms in stand-alone structures, it could be difficult to reliably incorporate them into periodically repeating unit cells, as a basis for an energy-absorbing mesostructure. A more promising approach is that of Qiu *et al.* [8], who showed that quazi-zero and negative stiffness can be obtained by fabricating a beam with a curved shape and then loading it transversely. No pre-compression or parallel, positive springs are required. The analytical model of the curved beam is described in Section 2. Section 3 describes additively manufacturing and testing prototype negative stiffness unit cells. In Section 4, the curved beams are used as the unit cell basis for a periodically repeating honeycomb mesostructure, and the performance of the mesostructure is simulated and described.

2. CURVED BEAMS AS NEGATIVE STIFFNESS ELEMENTS

In work related to micro-electromechanical systems (MEMS) switches, Qiu *et al.* [8] show that negative stiffness behavior can be generated by fabricating a beam with a curved shape, as described by Eq.(1),

$$\bar{w}(x) = \frac{h}{2}\left[1 - \cos\left(2\pi \frac{x}{l}\right)\right]. \tag{1}$$

In Eq. (1), $\bar{w}(x)$ is the average distance of the beam from the straight line connecting its two endpoints, h is the apex of the beam, x is the lateral position along the straight line connecting the beam's endpoints, and l is the beam span. Figure 5 depicts the geometric parameters of interest in the curved beam. The associated force-displacement relation of the curved beam shown in Figure 6 is given by

$$F = \frac{3\pi^4 Q^2}{2}\Delta\left(\Delta - \frac{3}{2} + \sqrt{\frac{1}{4} - \frac{4}{3Q^2}}\right)\left(\Delta - \frac{3}{2} - \sqrt{\frac{1}{4} - \frac{4}{3Q^2}}\right). \tag{2}$$

In Eq. (2), the normalized force, F, is given by the relation, $F = fl^3/(YIh)$, where f is the applied force, Y is the Young's modulus of the beam material, and I is the moment of inertia of the beam. The variable Q is a geometry constant and is given by the relation, $Q = h/t$, where t is the beam thickness. Finally, Δ is the normalized displacement and is given by the relation, $\Delta = d/h$, where d is the displacement in the transverse direction.

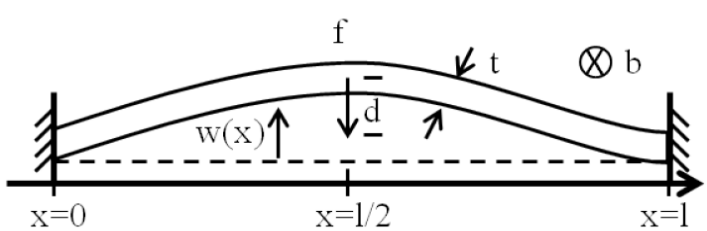

Figure 5. Geometry of a curved beam, adapted from Qui *et al.* [8]

Equation (2) can be used to design structures with desired force-displacement behavior, and thus, desired stiffness. For example, Figure 6 shows the force-displacement relations of beams with different Q values, given the properties contained in Table 1. Figure 6 shows both the normalized (panel (a)) and actual (panel (b)) force-displacement responses, and demonstrates the usefulness of Eq. (2) as a design tool for obtaining a specific response. For example, a beam with $Q = 1$ yields a monotonically-increasing force-displacement curve (i.e., strictly positive stiffness); when $Q \approx 1.2$, one observes an almost flat force-displacement curve (i.e., quasi-zero stiffness); and when $Q = 1.5$, a negative force-displacement slope (i.e., negative stiffness) is

observed. Note that while a beam with a $Q = 1.5$ exhibits negative stiffness, it is nevertheless mono-stable because any positive displacement results in a strictly positive force. For bistability to occur, the force must be less than zero for a particular range of positive displacements. Qiu et al. [8] point out that a beam with second-mode buckling constrained (which could be achieved, for example, by coupling it with another curved beam) will be bistable for Q > 2.31. Failure to limit the second-mode deformation prevents the beam from exhibiting sufficient NS to lead to bistability.

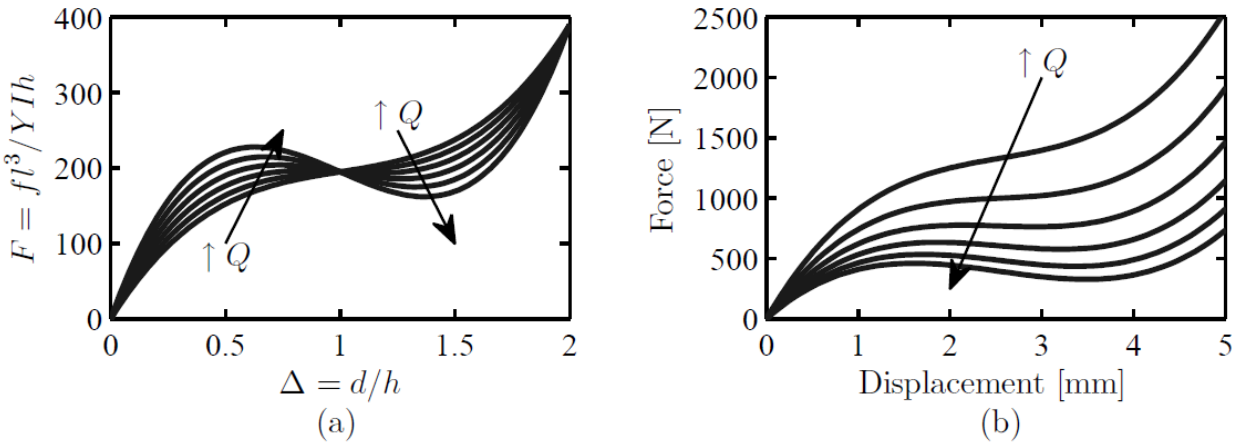

Figure 6. Force-displacement relation for a range of *Q* values from 1 to 1.5 in increments of 0.1: (a) normalized and (b) actual force and displacement values.

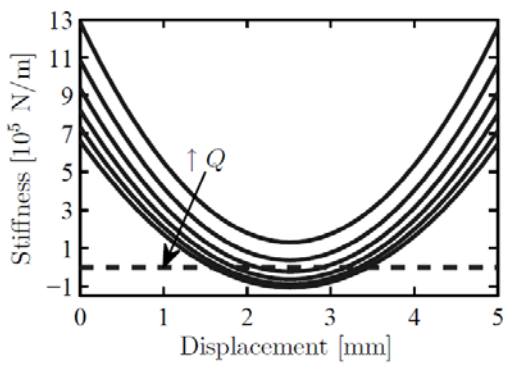

Figure 7. Stiffness vs. displacement for a range of *Q* values from 1 to 1.5 in increments of 0.1.

Property	Value
Y (GPa)	1.27
l (in)	1
h (in)	0.1
b (in)	1

Table 1. Beam design parameters for Figures 6 and 7.

The stiffness of a curved beam can be calculated as the first partial derivative of the force function with respect to displacement. The stiffness is calculated for a range of Q values and shown in Figure 7. The trends discussed in the preceding paragraph are clearly shown, as well as the observation that the nonlinear stiffness values asymptotically approach a certain stiffness value. There is a finite stiffness limit for a beam based on material properties and geometry related to the Q value.

3. Design, Fabrication, and Testing of Negative Stiffness Unit Cells

The experimental work presented here focuses on producing beams with low Q values as a proof of concept for the generation of NS elements by design. Equation (2) was used to generate the parameters for beams with desired stiffness. These beams were then integrated with a T-

shaped interface and a supporting frame, as shown in Figure 8, with the design parameters listed in Table 2.

FEA was performed on the single unit cell to validate the curved-beam approach for obtaining NS. The FEA results are compared with the analytical prediction in Figure 9. The results indicate strong agreement between the FEA and analytical predictions. Both the force- and stiffness-displacement responses are very similar between the analytical prediction and the FEA. The FEA considers a beam with elastic boundary conditions, whereas the analytical expression considers beams with fixed ends only. This difference is likely to be the primary source of discrepancy between the analytical and FEA model results.

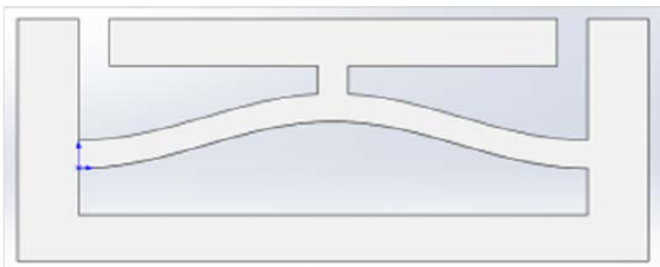

Figure 8. Solid model rendering of curved beam unit cell.

Property	Value
Y (GPa)	1.27
l (in)	1
h (in)	0.1
b (in)	1
Q	2

Table 2. Beam design parameters for Figures 8 through 12.

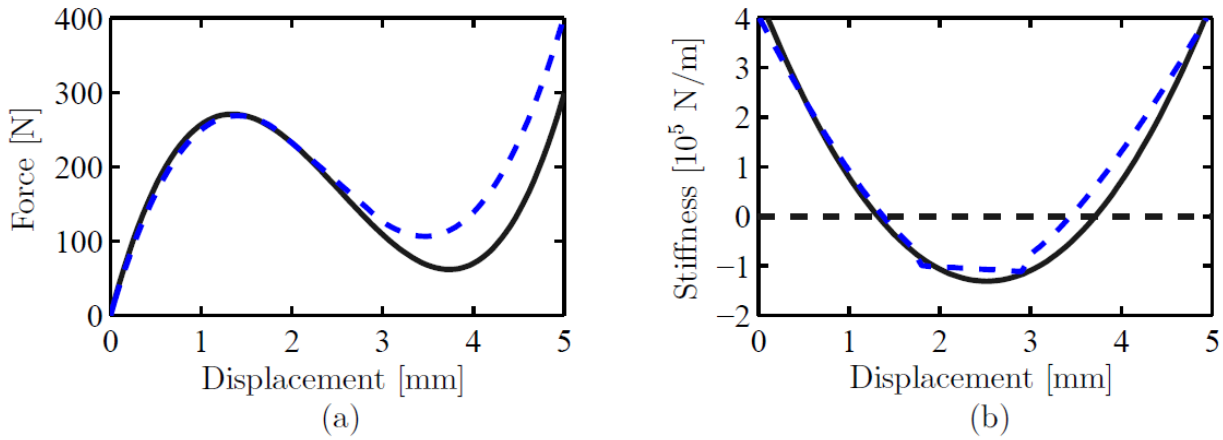

Figure 9. Comparison of analytical prediction (black solid line) and FEA (blue dotted line): (a) force-displacement and (b) stiffness displacement for the unit cell in Figure 8.

The unit cell was fabricated on an SLS HiQ Sinterstation Machine using Nylon 11 powder. The machine parameters are listed in Table 3. The resulting manufactured unit cell is shown in Figure 10. The force-displacement behavior of the unit cell was tested using an MTS Sintech 2/G test frame equipped with a 10,000 N load cell. As shown in Figure 10, a range of displacements was applied to the top of the T-shaped interface and the reaction force as a function of displacement was monitored by the load cell. This particular test stand is equipped with a bearing-mounted bottom platform which allows for self-righting of the platform. An aluminum block was fabricated to sit atop the T-shaped interface of the unit cell to ensure flatness with respect to the load cell. Finally, the NS element was mounted in a steel vise, which provided a zero-displacement boundary condition, when desired, at the edges of the NS element.

Figure 10 shows example deformations of the unit cell during testing with a constrained boundary condition applied to the edges. The large and nonlinear displacements of the beam element are evident as the displacement applied at the top of the element is increased. Force-displacement plots for zero-displacement and free boundary conditions are shown in Figures 11a and 11b, respectively. The black data points and arrows indicate the loading path (displacement applied downwards), and the blue data points and arrows indicate the unloading path. Figure 11a shows that with a constrained boundary condition, the large element exhibits NS over a range of displacements of approximately 1.75 to 3.5 mm. Furthermore, Figure 11 shows that the force-displacement relationship is highly repeatable (at least in the case of loading), even for different displacement amounts. Figure 11a shows that the unit cell has a different force-displacement relationship depending on the direction of loading. When the unit cell is unloaded after having been compressed, the results do not follow the loading curve. Furthermore, Figure 11a shows that for different displacements, the force-displacement relation differs on the unloading path. This is most likely due to internal material losses, which have been investigated experimentally in previous work with Nylon 11 SLS components [9].

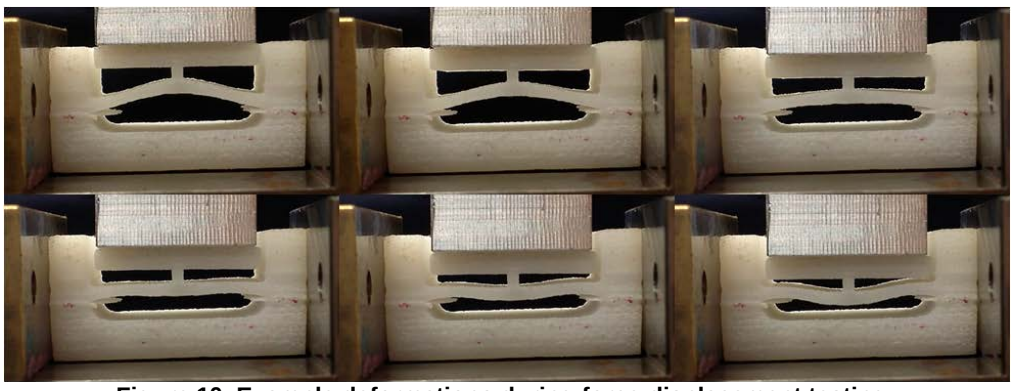

Figure 10. Example deformations during force-displacement testing.

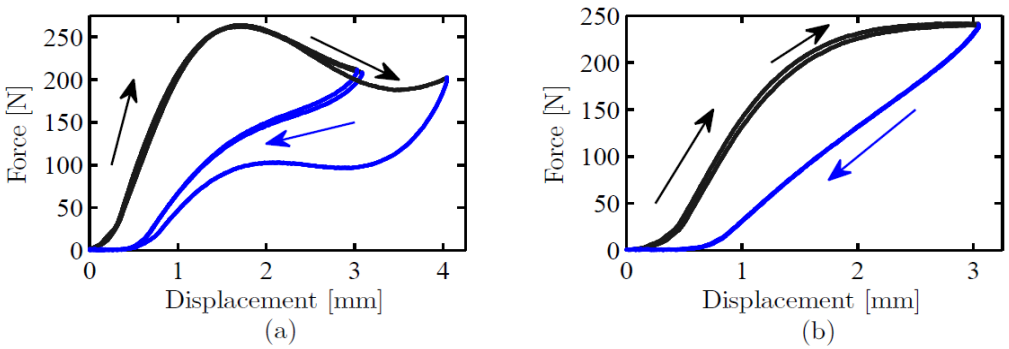

Figure 11. Experimental force-displacement curves for the curved beam unit cell with (a) zero-displacement and (b) free boundary condition. Black data points and arrows indicate results for the loading, and blue data points and arrows the unloading path.

Figure 11b depicts the effect of easing the constraints on the edges of the unit cell. With the boundary constraint free, the unit cell no longer demonstrates negative stiffness. This is a result of the increased flexibility of the unit cell frame at its boundaries leading to the elimination of the negative stiffness effect. Similar to Figure 11a, Figure 11b also demonstrates repeatable test results as well as different paths for loading and unloading.

FEA and experimental force-displacement curves are compared in Figure 12. Only the loading path is compared, because the FEA model did not incorporate material losses to model the full-cycle response. Although not an exact match, the FEA results reflect distinct similarities with the test data. Negative stiffness behavior is observed with zero-displacement boundary conditions for FEA and experimental conditions, and it occurs over a similar range of displacements at a similar force threshold. Also, the loading path is similar for FEA and experimental conditions with free boundary conditions. Discrepancies between experimental and FEA data are most likely caused by imprecision in the SLS manufacturing process. A few spot-check measurements of the as-built dimensions of the prototype unit cells revealed differences from the as-designed dimensions. For example, whereas the curved beam was designed with a constant thickness, t, the as-built elements demonstrated a non-constant thickness, whose effects on force-displacement behavior are difficult to quantify.

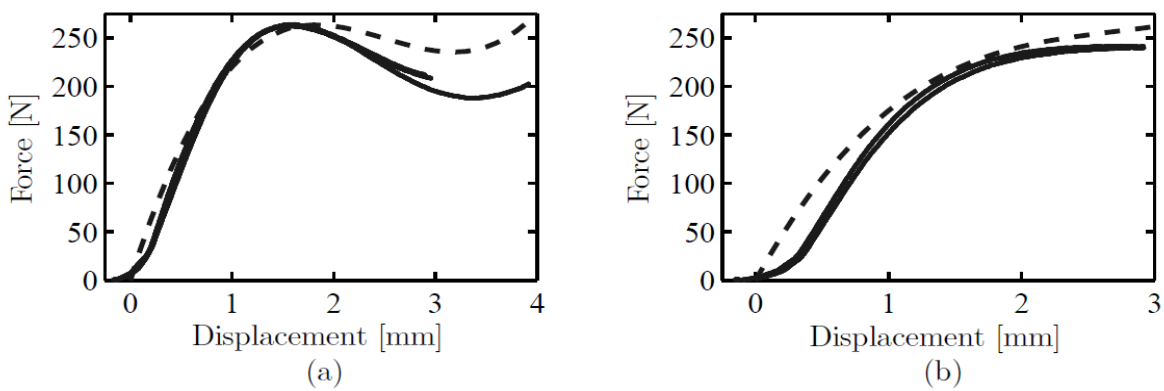

Figure 12. Comparison of experimental (loading path only) and FEA force-displacement curves for (a) zero-displacement and (b) free boundary conditions. FEA results are plotted with dashed black lines and experimental data with solid black lines.

4. Designing and Modeling Periodically Repeating, Negative Stiffness Mesostructures

The next step is to design negative stiffness mesostructures by periodically repeating an appropriate unit cell. The basic concept is illustrated in Figure 13. As shown in the figure, the shock absorbing mesostructure is composed of negative stiffness, curved beam structures (A) that undergo large displacements while transiting a region of negative stiffness upon application of a load (B) and then return to their initial state when the load is removed (C). Figures 13 D, E, and F illustrate a magnified view of a single curved beam element as it is loaded and unloaded. The unit cell is Figure 13 was modified to alleviate stress concentrations in the joints; and the new unit cell is illustrated in Figure 14. As shown in Figure 14a, the unit cell is composed of two curved beams, each of which yields negative stiffness behavior.

The first step in investigating the performance of the mesostructure is to model the behavior of its unit cells. Some of the basic dimensions for a unit cell are illustrated in Figure 15. The force-displacement relationships for a partial unit cell and for two unit cells are illustrated in Figures 16 and 17, respectively. These force-displacement relationships are derived from FEA models that apply symmetric boundary conditions to the left and right sides of each geometry and displacement-controlled loading to the top of the geometry. As shown in Figure 16, the

curved beam geometry yields negative stiffness behavior, illustrated by the negative slope in Figure 16. As shown in Figure 17, each additional row of curved beams in the mesostructure yields an additional region of negative stiffness, as the rows of curved beams progressively encounter regions of negative stiffness. It is also important to note that the force threshold at which the negative stiffness behavior occurs can be tailored by adjusting the beam geometry and the number of columns of unit cells. As shown in Figures 16 and 17, by adding a second row of unit cells, the force threshold doubled from approximately 40 N to approximately 80 N. Furthermore, the displacement of the mesostructure prior to densification is directly proportional to the number of rows of curved beams, with the total displacement doubling from Figure 16 to Figure 17 as the number of rows doubles.

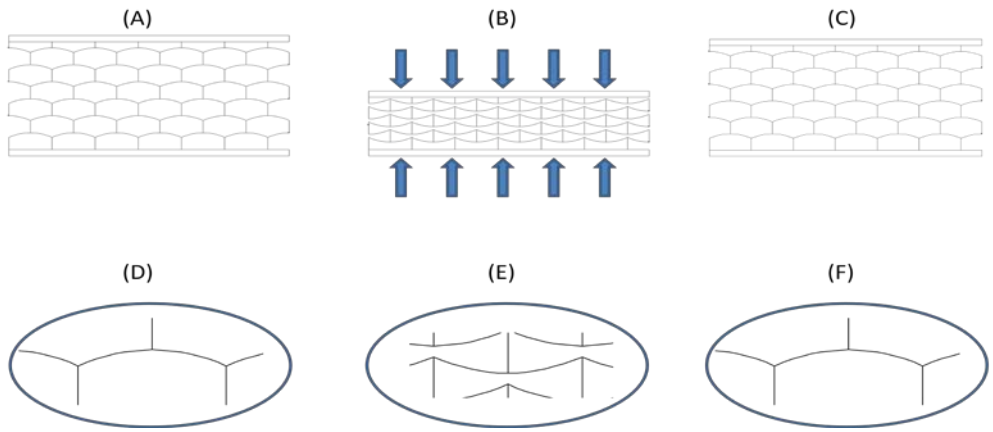

Figure 13. A negative stiffness mesostructure (a and d), capable of absorbing energy at a particular force threshold (b and e) and then recovering its original configuration (c and f) in preparation for the next loading event.

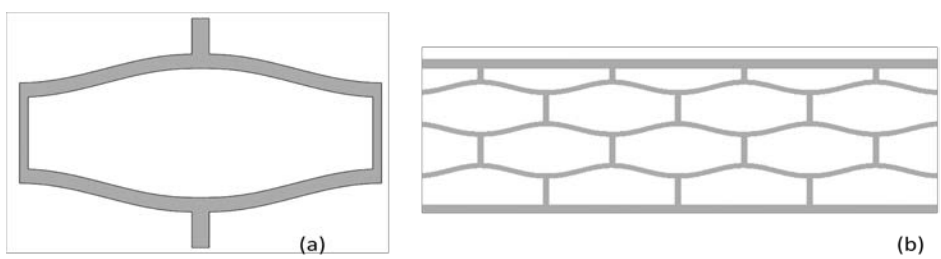

Figure 14. A negative stiffness unit cell composed of two curved beams (a) and periodically repeated to form a negative stiffness mesostructure (b).

Figure 18 compares the performance of the curved beam mesostructure to that of standard square and hexagonal cell mesostructures with equivalent relative densities. From this plot, it is clear that the in-plane effective elastic stiffness of the curved beam mesostructure is nearly identical to that of the hexagonal mesostructure. The force or stress threshold at which buckling occurs is very similar in the two designs, as well. The primary difference is that the hexagonal mesostructure transitions from elastic deformation to plastic buckling, whereas the curved beam mesostructure transitions to the negative stiffness regime which subjects the cell walls to elastic buckling and extension/compression. Therefore, the curved beam mesostructure absorbs energy in a recoverable way, such that it can reset to its original configuration when the load is removed,

in preparation for the next loading event. The hexagonal mesostructure, in contrast, undergoes permanent cell buckling, collapse, and densification.

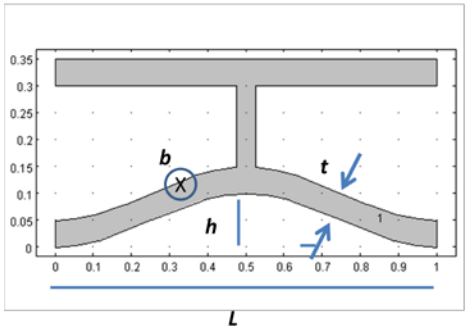

Beam parameter	Value
Length, L	1 m
Apex, h	.1 m
Thickness, t	.05 m
Q (h/t)	2
Depth, b	.1 m
Young's modulus, E	1.27 GPa
Poisson's ratio, v	.33
Density	975 kg/m^3

Figure 15. Dimensions and material properties for FEA simulations of the negative stiffness mesostructure.

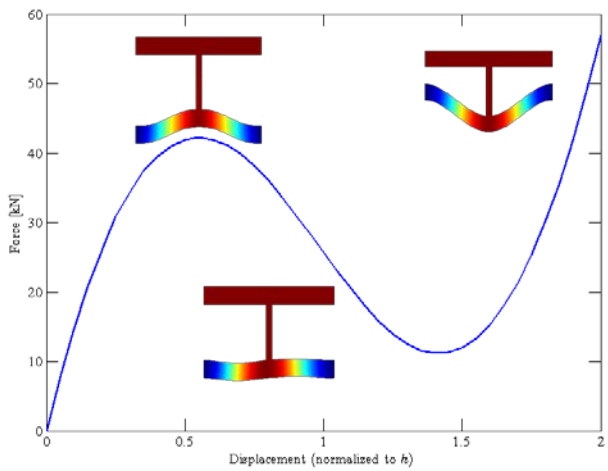

Figure 16. Force-displacement relationship for a single curved beam with the dimensions documented in Figure 15.

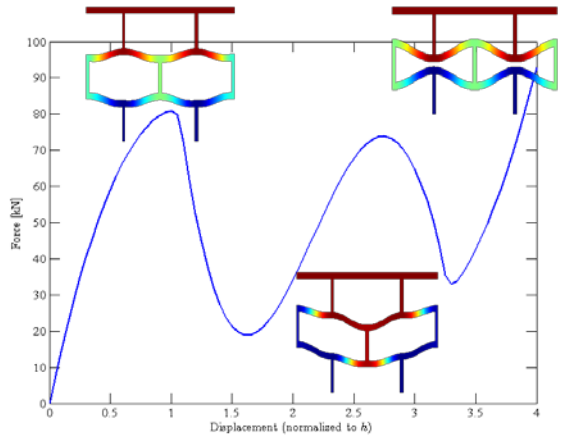

Figure 17. Force-displacement relationship for a double unit cell.

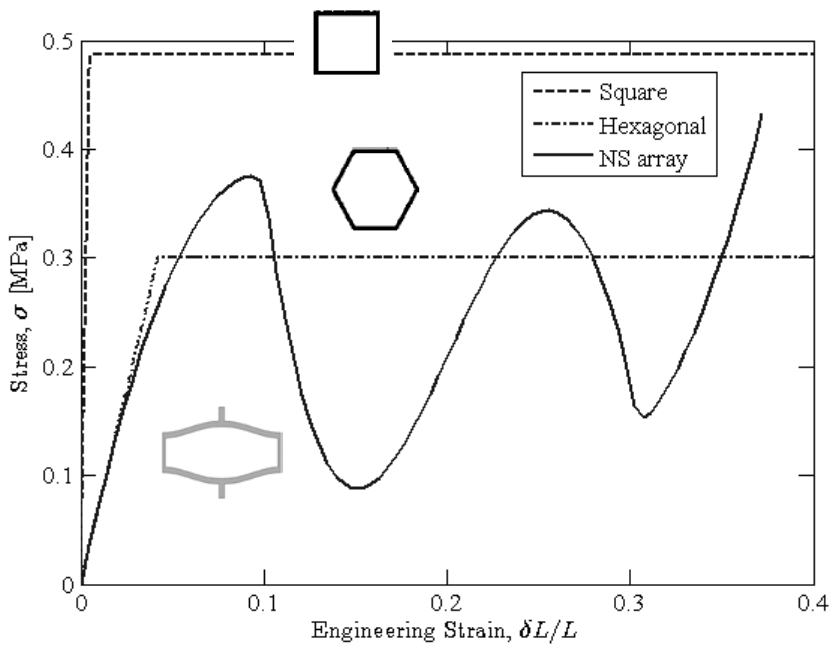

Figure 18. Comparison of the stress-strain behavior of the negative stiffness mesostructure to square and hexagonal honeycombs, all with equivalent relative density of 15%.

5. CLOSURE

The negative stiffness mesostructure presented in this paper is a new shock-isolating cellular structure for absorbing transient mechanical loads. Unlike traditional honeycombs, the proposed cellular structure would be self-settable, and therefore reusable, and be optimized for specific shock events. Application-specific customization could be achieved by functionally tailoring the geometry of the unit cells and fabricating them using additive manufacturing techniques, such as selective laser sintering. Although higher in initial manufacturing cost than traditional

honeycombs, the reusability aspect of the proposed design could lead to significant cost savings relative to one-time use honeycombs; and the customizable, nearly-ideal shock isolation aspect could lead to enhanced levels of isolation from specific shock events. Further, the recoverable deformations may enable energy absorbing behavior in the event that subsequent loading events follow the initial load.

Further work is needed to fabricate these negative stiffness mesostructures and experimentally evaluate their force-displacement behavior. Specifically, the negative stiffness behavior of the curved beam mesostructure tends to be sensitive to its boundary conditions—a phenomenon that needs to be experimentally investigated. Also, robust negative stiffness behavior relies on a transition from first to third to first mode buckled shapes as the curved beams are loaded, whereas second mode buckling shapes may appear in these curved beams, especially if the additive manufacturing process induces some imperfections in the geometry or material properties. Modifications may be required to the cell structure to impose a third mode buckling shape as the curved beam transitions from one first mode buckling shape to another. Finally, it is possible to tailor the mesostructure from row to row, such that each row of cells reacts to a different force threshold, resulting in a cascading series of shock isolating events.

ACKNOWLEDGEMENTS

The authors gratefully acknowledge support from the Defense Advanced Research Projects Agency, Strategic Technology Office (STO), under the Structural Logic program managed by Dr. Aaron Lazarus, under contract number HR0011-10-C-0125. The views and conclusions contained in this document are those of the authors and should not be interpreted as representing the official policies, either expressly or implied, of the Defense Advanced Research Projects Agency or the U.S. Government.

REFERENCES

1. Gibson, L. J. and M. F. Ashby, 1997, *Cellular Solids: Structure and Properties*, Cambridge University Press, Cambridge, UK.
2. Hayes, A. M., A. Wang, B. M. Dempsey and D. L. McDowell, 2004, "Mechanics of Linear Cellular Alloys," *Mechanics of Materials*, Vol. 36, No. 8, pp. 691-713.
3. Balandin, D. V., N. N. Bolotnik and W. D. Pilkey, 2001, *Optimal Protection from Impact, Shock, and Vibration*, Taylor and Francis, Philadelphia, PA.
4. Kent, R. W., D. V. Balandin, N. N. Bolotnik, W. D. Pilkey and Purtsezov, 2007, "Optimal Control of Restraint Forces in an Automobile Impact," *Journal of Dynamic Systems, Measurement, and Control*, Vol. 129, pp. 415-424.
5. Barry Controls Department, Accessed April 22, 2012, "Passive Shock Isolation," *www.barrycontrols.com/uploads/tech/PassiveShock.pdf*.
6. Seepersad, C. C., J. K. Allen, D. L. McDowell and F. Mistree, 2006, "Robust Design of Cellular Materials with Topological and Dimensional Imperfections," *ASME Journal of Mechanical Design*, Vol. 128, No. 6, pp. 1285-1297.
7. Zhou, N. and K. Liu, 2010, "A Tunable High-Static-Low-Dynamic Stiffness Vibration Isolator," *Journal of Sound and Vibration*, Vol. 329, pp. 1254-1273.
8. Qiu, J., J. H. Lang and A. H. Slocum, 2004, "A Curved-Beam Bistable Mechanism," *IEEE Journal of Microelectromechanical Systems* Vol. 13, No. 2, pp. 137-146.

9. Kashdan, L., 2010, "Evaluation of Negative Stiffness Elements for Enhanced Material Damping Capacity," *M.S. Thesis,* Mechanical Engineering Department, The University of Texas at Austin, Austin, TX.